Medical Engineering and Physics 000 (2017) 1–8

Contents lists available at ScienceDirect

Medical Engineering and Physics

journal homepage: www.elsevier.com/locate/medengphy

Three-dimensional computational model of a blood oxygenator reconstructed from micro-CT scans

C. D'Onofrio[a,*], R. van Loon[a], S. Rolland[a], R. Johnston[a], L. North[a], S. Brown[b], R. Phillips[b], J. Sienz[a]

[a] Swansea University, College of Engineering, Swansea SA1 8EN, UK
[b] Institute of Life Science 2, Haemair Ltd., Swansea SA2 8PP, UK

ARTICLE INFO

Article history:
Received 12 May 2016
Revised 7 June 2017
Accepted 14 June 2017
Available online xxx

Keywords:
ECMO
Hollow Fibre Membrane
Non-Newtonian
Blood
Micro-CT

ABSTRACT

Cardiopulmonary bypass procedures are one of the most common operations and blood oxygenators are the centre piece for the heart-lung machines. Blood oxygenators have been tested as entire devices but intricate details on the flow field inside the oxygenators remain unknown. In this study, a novel method is presented to analyse the flow field inside oxygenators based on micro Computed Tomography (μCT) scans. Two Hollow Fibre Membrane (HFM) oxygenator prototypes were scanned and three-dimensional full scale models that capture the device-specific fibre distributions are set up for computational fluid dynamics analysis. The blood flow through the oxygenator is modelled as a non-Newtonian fluid. The results were compared against the flow solution through an ideal fibre distribution and show the importance of a uniform distribution of fibres and that the oxygenators analysed are not susceptible to flow directionality as mass flow versus area remain the same. However the pressure drop across the oxygenator is dependent on flow rate and direction. By comparing residence time of blood against the time frame to fully saturate blood with oxygen we highlight the potential of this method as design optimisation tool.

In conclusion, image-based reconstruction is found to be a feasible route to assess oxygenator performance through flow modelling. It offers the possibility to review a product as manufactured rather than as designed, which is a valuable insight as a precursor to the approval processes. Finally, the flow analysis presented may be extended, at computational cost, to include species transport in further studies.

1. Introduction

According to the National Health Service (NHS [19]) and Health and Safety Executive (HSE [10]), up to 25,000 people die of Chronic Obstructive Pulmonary Disease (COPD) every year and the disorder affects over a million individuals in Great Britain. In addition up to 400 people develop Acute Respiratory Distress Syndrome (ARDS) with a mortality rate of over 50%. Improving treatment techniques have a direct social and individual impact in saving lives, increasing life expectancy and reducing cost to the public health services. Two different methods are clinically approved and are used to transfer oxygen into the blood:

- Mechanical ventilation, mainly controlled by pressure and/or volume (Chatburn et al. [4]), transfers oxygen into the lungs of the patient for the gas exchange. Often the ventilation pressure and oxygen concentration are set very high to overcome the impaired lung function. A potentially resulting barotrauma, volutrauma and oxygen toxicity may prevent or slow down the lung recovery.
- Extra Corporeal Membrane Oxygenation (ECMO) is bypassing the cardiopulmonary cycle by oxygenating the blood outside the patient by pumping blood through a bed of micro-porous Hollow Fibres Membranes (HFM). For details on the development of ECMO, the reader is referred to Haworth [8].

For the last decade ECMO devices based on HFM prevailed and has brought a new branch of studies, where the oxygenator itself is investigated. The oxygenator is one of the centre pieces of the ECMO circuit and the development of hollow fibres with membranes or micro porous walls is advancing rapidly with novel materials and coatings. The effort to optimize the HFM-assembly concentrates to reduce the pressure drop across the device, to minimize haemolysis, decrease the priming volume of blood, and increase biocompatibility and lifetime of HFM oxygenators.

Computational fluid dynamic (CFD) models are used to study blood flow path, heat exchange, pressure drop, stress analysis,

* Corresponding author.
E-mail address: c.donofrio@swansea.ac.uk (C. D'Onofrio).

http://dx.doi.org/10.1016/j.medengphy.2017.06.035

mass transfer of oxygen and carbon dioxide, different convection-diffusion models, blood stagnation, thrombogenicity, etc. These models use either a homogeneous porous media to describe the fibre bundle in bulk or a heterogeneous approach to model single fibre arrangements. The rheology is usually implemented as Newtonian flow field or more realistically described as shear thinning fluid. Non-Newtonian shear thinning numerical models for blood are well known and described by Johnston et al. [11] or Marcinkowska-Gapińska et al. [15].

For example Gartner et al. [6] and Pelosi et al. [20] use a porous media approach to model thrombogenic depositions and study the thrombogenic potential of oxygenators. Zhang et al. [25] predict blood-gas exchange and pressure drop with a Newtonian flow field through a porous media. A comparison of different porous media models is presented by Khanafer et al. [13] with a set porosity ($\Phi = 0.75$). Hormes et al. [9] present a novel diffusivity model to predict the O_2 and CO_2 mass transfer and partial pressure, which is validated by comparing the numerical solution with a purpose built oxygenator. The oxygenator and the CFD model use a uniform distribution of fibres.

Commonly the same partial pressure P_{O_2} is applied at the fibre surface for convection and diffusivity. Taskin et al. [23] presented a novel model to describe gas exchange as profile on the fibre surface. The study is comparing a single and multi fibre approach with uniform fibre distribution.

A study by Nagase et al. [18] presented mass transfer correlations based on the theory for heat transfer across a tube bank and concluded that the mass transfer performance of membrane oxygenators is attributable to the hollow fibre arrangement. The layouts considered are uniformly arranged staggered or squared (inline) fibres.

An oxygenator cross-section modelled with individual fibres in two dimensions is compared to the porous media approach by Mazaheri and Ahmadi [16]. To avoid computational costly simulations of individual fibres, novel porous models are developed to integrate the fibre distribution for a better local process mapping (Low et al. [14], Zhang et al. [25]) and an attempt to "adjust" the porosity based on fibre orientation is described by Bhavsar et al. [3].

But all off these models have been developed with the assumption of a uniform distribution of fibres either staggered, squared or crossed (3D) or simplified with a porous media approach. Although a good agreement between numerical predictions and experimental results has been reported in the literature by Consolo et al. [5] and Pelosi et al. [20], the porous media approach is inherently unable to capture and characterize the intricate details on the flow field within the fibre bundles.

Imaging modalities can be used as a diagnostic tool to investigate the micro-structural components in an oxygenator and, when combined with CFD, can even provide information on the localised functional behaviour (flow/oxygenation) of the device. In this paper we demonstrate a method for building a full-scale, image-based, three-dimensional computational model of a blood oxygenator. All individual fibres are reconstructed from the images of a μCT scan and CFD is performed using a Non-Newtonian fluid model to investigate the local flow field inside the device.

2. Prototypes and methods

The common method of extra-corporeal oxygenating blood is achieved by pumping ambient air or through the core of HFM's whereas the blood is flowing on the outside of the fibres. Molecular diffusion increases the oxygen level in the red blood cells and removes carbon dioxide from the venous blood.

Fig. 1. Image of an oxygenator prototype (SRD3083), courtesy of Haemair Ltd. For this experiment, blood flows from the inlet A to the outlet B.

2.1. Prototypes

Two manually assembled oxygenators are used for experimental evaluation. The blood samples, outdated packed cells, are sourced from the Welsh Blood Service [24] which is accredited by the Medicines and Healthcare products Regulatory Agency [7]. The experiments are conducted by Haemair Ltd. and follow their standard of operation procedure SOP2007v04. One of the prototypes is depicted in Fig. 1. The core of the oxygenator is built with folded mats of hollow fibres produced by Membrana GmbH [17]. The fibres are state of the art ('OXYPLUS®') and have an outer diameter of approximately 380 µm and a nominal wall thickness of 90 µm. The fibre wall is highly porous ($\geq$ 55%) to allow molecular diffusion but blocking any fluid. For more details see Membrana GmbH [17]. Resin seals both ends of the oxygenator around the fibres, forcing the blood to flow between inlet and outlet (Fig. 1). Ambient air is pumped through the hollow core of the fibres. The nominal outer dimensions of the enclosure is 10 × 20 × 100 mm. Both prototypes are built to support flow along the fibres and to prevent cross-flow between the fibres at the same time, to minimize clotting and haemolysis. Additionally a virtual idealised geometry is used to set up the CFD model. Size, volume and fibre count are comparable to the real world devices. The fibres in the virtual device are uniformly arranged to exploit symmetry and simplify meshing. The virtual model is used for comparison and to test the numerical solution. For all devices the key characteristics are listed in Table 1.

2.2. Reconstructed geometry

μCT scans were performed on both prototypes using a Nikon XT H 225 with a voxel size of 22 µm. The source voltage and current were set to 55 kV and 174 µA, respectively. The exposure time for each radiograph was 2 s, with 720 radiographs being collected over 360 °.

A complete set of reconstructed two-dimensional images was computed with ~1500 × 1000 pixels and a displacement in z-direction of ~30 µm. The images captured from the μCT scan show the fibres and their arrangement in great detail (see Fig. 2). The warp thread in OXYPLUS® mats is a polyethylene terephthalate (PET) multifilament yarn (33 dtex[1]) with 24 filaments. The threads, with an estimated diameter of ~70 µm± 10, are woven into the fibre bundle every 10 mm to keep the fibres at a minimum distance and hence allow blood flow in-between. Due to the small size of the threads, we assumed that any pressure drop or mixing affects can be neglected for this study. To verify that the fibres remain in a straight line (in z-direction, see Fig. 4) throughout the device a visual inspection was conducted on a 3D compilation [22] of the μCT images (see Fig. 2) as well as overlaying 2 images from the opposite ends. A cross-section image for each oxygenator (Fig. 3a and b) was used to recreate a full size real world three-dimensional geometry to run CFD-simulations. Both prototypes were manually

[1] Dtex (decitex) is a textile measuring unit for yarn. 1 dtex = 0.1 g/km.

Please cite this article as: C. D'Onofrio et al., Three-dimensional computational model of a blood oxygenator reconstructed from micro-CT scans, Medical Engineering and Physics (2017), http://dx.doi.org/10.1016/j.medengphy.2017.06.035

Table 1
Characteristics of oxygenators.

	Var	Idealised	SRD3078	SRD3083	
Width (mm)	w	17.11	19.20	18.92	
Height (mm)	h	8.63	9.87	9.70	
Length (mm)	l	100	100	100	
Inlet/Outlet diameter (mm)		3	3	3	
Inlet/Outlet length (mm)		20	20	20	
Fibre wall thickness (µm)	T_f	90	90	90	±10 µm
Fibre outer diameter (µm)	D_{fo}	380	380	380	±30 µm
Fibre inner diameter (µm)	D_{fi}	200	200	200	Nominal
Fibre count (n)	N_f	512	508	531	
Fibres merged (n (%))		0 (0)	7 (1.4)	8 (1.5)	
Surface area fibres (mm^2)	A_f	61,122.8	60,645.3	63,391.1	$\pi \times D_{fo} \times 10^{-3} \times l \times N_f$
Device volume (mm^3)	V_d	14,765.93	18,950.4	18,352.4	$w \times h \times l$
Fibre volume (mL)	V_f	5.8067	5.7613	6.0222	$\pi \times (\frac{D_{fo}}{2})^2 \times l \times N_f \times 10^{-9}$
Static priming volume (mL)	V_b	8.9593	13.1891	12.3302	$(V_d \times 10^{-3}) - V_f$
Gas volume (mL)	V_g	1.6085	1.5959	1.6682	$\pi \times (\frac{D_{fi}}{2})^2 \times l \times N_f \times 10^{-9}$
Blood volume oxygenated (mL)	V_{b*}	0.6273	0.6224	0.6506	Eq. (4), $d = 10\,\mu$m
Porosity (%)	Φ	60.68	69.60	67.19	$\frac{V_b}{V_d \times 10^{-3}}$
V/Q ratio (%)		17.95	12.10	13.53	$\frac{V_g}{V_b}$
V/Q ratio oxygenated (%)		256.41	256.41	256.41	$\frac{V_g}{V_{b*}}$

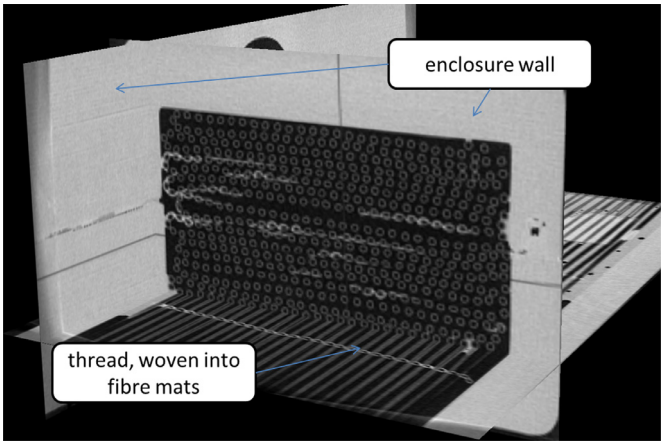

Fig. 2. Sliced 3D model reconstructed from μCT 2D images including a thread woven in to maintain a minimum distance between the fibres.

assembled by folding HFM mats into the plastic enclosure. The device SRD3083 has added spacers (see Fig. 4) between the folds to support a uniform distribution of fibres throughout the device. The spacers are 100 µm thick and are completely embedded in the resin sealed ends.

2.3. Modelling technology and mesh dependency

We use the cell centre based finite volume formulation to solve the incompressible Navier–Stokes equation for momentum and mass conservation. The blood flow through the devices is modelled with ANSYS Inc. [1]—FLUENT. The solver was set for a pressure-based steady state solution with absolute velocity. The problem was discretised using a least-square cell based gradient formulation combined to a second order upwind discretisation scheme for momentum and a second order scheme for pressure. The SIMPLE algorithm was used for pressure coupling. A representative section of fibres from the device SRD3078 was used to build a smaller version of blood oxygenator with a manually refined mesh with approximately 2 million elements. A grid convergence study was conducted to find a suitable set of parameters to create an appropriate unstructured mesh for all devices. With a minimum size restriction for elements set to 1×10^{-6} m and a biased sweep mesh for the main body, we have a confidence level of ±2% error in regards to pressure drop for the numerical solution. To limit the amount of elements further, a minimum gap size of ≧10 µm is imposed between individual fibres or between fibres and enclosure. This is achieved by merging fibres or joining fibres with the enclosure wall if the gap is smaller (see Fig. 5). A total of 7 fibres are merged for the device SRD3078 and 8 fibres for the device SRD3083. For all meshes a minimum of five elements is enforced between the fibres. All three geometries have a final unstructured mesh with ~20 million cells. The inlet and outlet (ϕ 3 mm) tube length is set to 20 mm to support a fully developed fluid flow entering the oxygenator. The outlet is configured as pressure outlet and is set to 0 Pa and the fibres and the enclosure are defined as no-slip walls.

2.4. Simulation and visualisation of blood flow

A study comparing three rheological models (Casson, Ree-Eyring and Quemada [15]) concluded that the Quemada model fitted most precisely with their experimental findings. To solve the blood flow as incompressible Non-Newtonian fluid, the model (Quemada [21], Eq. (1)) is implemented as a user defined function

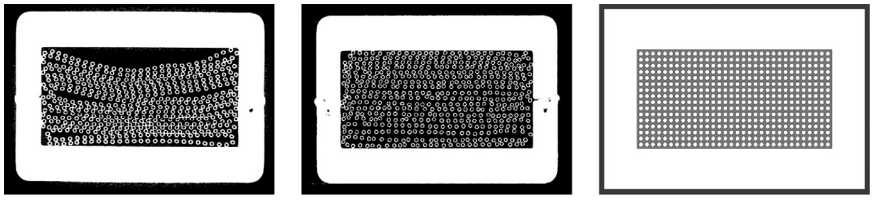

(a) SRD3078 (b) SRD3083 (c) ideal

Fig. 3. (a,b) μCT images of a cross-section for two manually assembled blood oxygenator prototypes. (b) Spacers between the folds help to create a more uniform distribution of fibres. (c) Idealised CFD-geometry to provide a comparable device with uniformly distributed fibres.

Please cite this article as: C. D'Onofrio et al., Three-dimensional computational model of a blood oxygenator reconstructed from micro-CT scans, Medical Engineering and Physics (2017), http://dx.doi.org/10.1016/j.medengphy.2017.06.035

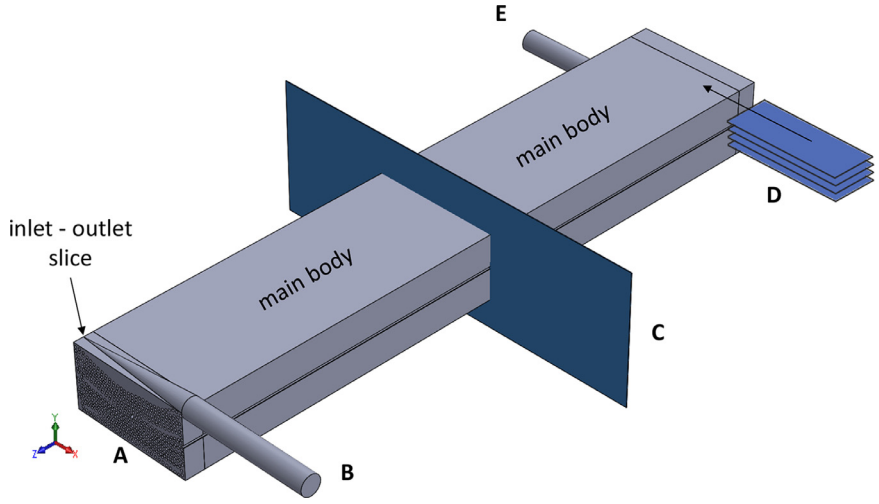

Fig. 4. (A) Reconstructed fibre distribution for SRD3078. (B,E) Inlet/outlet tube for blood. (C) Representation of "mid plane cross-section" to extract results, see Fig. 7. (D) "Spacers" inserted on both ends for the device SRD3083 to support a uniform distribution of fibres (cf. Fig. 3a and b).

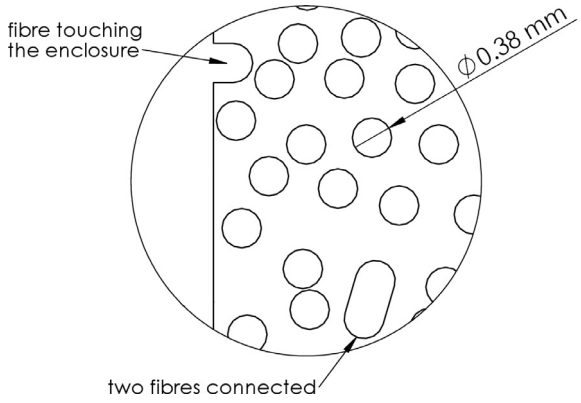

Fig. 5. Fibres joined together or merged with the enclosure where the gap size is $< 10\,\mu$m.

Table 2
Quemada model coefficents.

μ_p	1.23 mPa s	Blood plasma viscosity
H_{ct}	48 %	Haematocrit
k_0	3.96	Model constant for zero shear rate
k_∞	1.71	Model constant for infinite shear rate
$\dot{\gamma}_c$	5.0	Characteristic rate of rouleaux formation/degradation

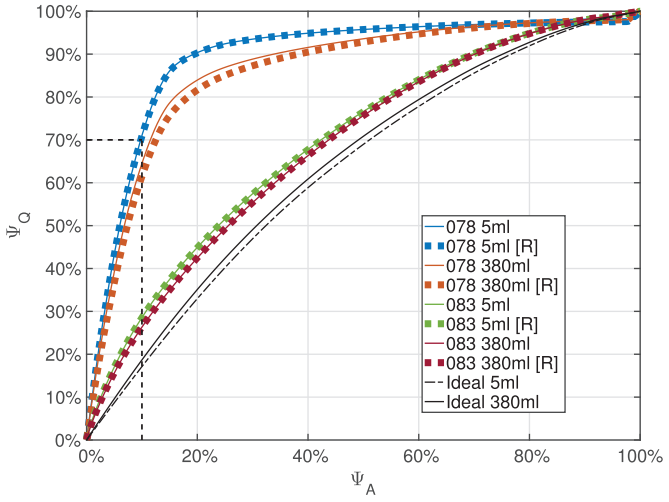

Fig. 6. Comparing area versus mass flow of blood for each device at the mid plane cross-section (I/2). Coloured solid lines represent forward flow, coloured dotted lines represent the [R]everse flow. For the idealised geometry the two mass flow rates (5 mL min^{-1} and 380 mL min^{-1}) are plotted in black with no reverse flow, since the geometry is symmetrical. (For interpretation of the references to colour in this figure legend, the reader is referred to the web version of this article.)

to report shear dependent viscosity. Parameters for deriving the viscosity μ are based on the work of Marcinkowska-Gapinska et al. [15] and listed in Table 2. Shear strain rate, denoted as $\dot{\gamma}$ is obtained from the flow field and the density is set to 1050 kg m^{-3} for average whole blood. With the above, viscosity can be described as

$$\mu = \frac{\mu_p}{(1 - \frac{1}{2} k_Q * H_{ct})^2} \quad \text{with } k_Q = \frac{k_0 + k_\infty \sqrt{\frac{\dot{\gamma}}{\dot{\gamma}_c}}}{1 + \sqrt{\frac{\dot{\gamma}}{\dot{\gamma}_c}}}. \tag{1}$$

The boundary condition for the blood flow is set as mass flow rate to 8.75×10^{-5} kg s^{-1} (5 mL min^{-1}) and 6.65×10^{-3} kg s^{-1} (380 mL min^{-1}), respectively. Two flow rates were chosen for modelling: the low Reynolds number regime was used as a laminar regime validation and a higher flow rate was used for direct comparison with experiments under conditions relevant to the devices' usage. For both prototype oxygenators the flow is simulated in both directions (reversing the inlet and outlet), with otherwise the same boundary conditions and parameters applied. The idealised geometry is symmetrical, hence there is no need to calculate the reverse flow for comparison.

To visualise mass flow versus area (Fig. 7) an ANSYS plug-in 'MassFlowAreaRatio' was developed to interrogate the results interactively. The plug-in is using the built-in API to Perl and the Power Syntax from CFX-Post (ANSYS CFX Reference Guide release 14.5) and allows to set arbitrary numbers of cross-sections in any direction with a pre-defined threshold for mass flow. Each step of the integration may be saved and stacks of images can be automatically saved to create an animation (see supplementary videos online–10.1016/j.medengphy.2017.06.035).

2.5. Oxygenator shunt fraction

Perfusion mismatch or impaired lung function is usually calculated using the Berggren Equation for shunt fraction (Q_s/Q_t [2]) to express the ratio of blood bypassing oxygenation (Q_s) to the total cardiac output (Q_t). In this study we use a similar approach to de-

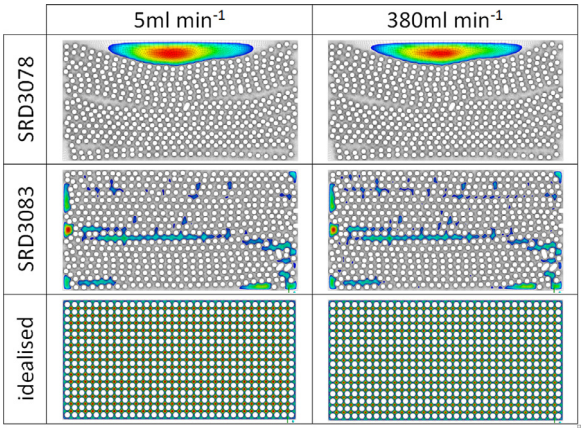

Fig. 7. Snap-shot of simulated mass flow (70%) at the mid-plane cross-section ($l/2$) for SRD3078 (top), SRD3083 (middle), and the idealised geometry (bottom), for a flow rate of 5 mL min^{-1} (left) and 380 mL min^{-1} (right), respectively. The colours are for a better visualisation only, and may not be compared between the different devices and flow rates (see supplementary videos online—10.1016/j.medengphy.2017.06.035). (For interpretation of the references to colour in this figure legend, the reader is referred to the web version of this article.)

fine the Oxygenator Shunt Fraction O_{sf} (Eq. (2)) as ratio of blood volume bypassing oxygenation.

$$O_{sf} = 1 - \frac{V_{b^*}}{V_b} \tag{2}$$

The blood being oxygenated is defined as V_{b^*} and is derived in Eq. (3) and rearranged in Eq. (4). In essence it describes the volume of annuli with thickness d around the fibres. See Table 1 for parameters length (l), count of fibres (N_f) and priming volume V_b.

$$V_{b^*} = l \times N_f \times \pi \times \left(\left(\frac{D_{fo}}{2} + d \right)^2 - \left(\frac{D_{fo}}{2} \right)^2 \right) \tag{3}$$

$$= l \times N_f \times \pi \times d \times (D_{fo} + d) \tag{4}$$

Assuming that only blood within a distance of $d = 10\,\mu$m to the outer fibre wall is active in gas exchange (approximately the size of human capillaries), Eq. (2) is used to find the ratio of blood not being exposed to the hollow fibre membrane and hence bypassing the oxygenation. O_{sf} is only valid for non-turbulent flow regimes with a perfect flow in longitudinal direction (z).

2.6. Cross flow ratio coefficient

The presented oxygenator prototypes have been built to support flow along the fibres to minimize clotting and haemolysis as well as to study flow rate and residence time. The goal is a perfect flow in longitudinal direction z (parallel to the fibres) in order to reduce priming volume and minimise residence time with complete oxygen saturation of the blood. Due to an asymmetrical arrangement of inlet and outlet, as well as a deviation from a uniform fibre distribution in the prototypes, we propose to use the coefficient O_{cf} (Eq. (5)) to quantify the amount of cross-flow present. u_i, v_i, w_i [ms^{-1}] are the three-dimensional components of the velocity vector at grid element i with count of all elements denoted by n. O_{cf} is dimensionless and describes the mean deviation from longitudinal flow-direction (z).

$$O_{cf} = \frac{1}{n} \sum_{i=1}^{n} \frac{\sqrt{u_i^2 + v_i^2}}{\sqrt{u_i^2 + v_i^2 + w_i^2}} \tag{5}$$

3. Results

As shown in Figs. 2 and 3, the images reconstructed from the μCT scan represent the oxygenator and the individual fibres in great detail. This allows to rebuild an accurate three-dimensional geometry with a CAD software which subsequently can be used to set up a CFD model. A visual inspection of two cross-section images from opposite ends and of slices of the 3D reconstruction shows very little deviation of the fibres in longitudinal direction (z). The spacers built into SRD3083 increase the uniformity of the fibre distribution significantly.

A two-dimensional cross-section plane is defined at position $l/2$ and for each cell in the mesh, mass flow and area are extracted and plotted (see Fig. 6). A formal description is found in Eq. (6). If Q_{bc} is the prescribed mass flow rate through the device and A_{CS} is the cross-sectional area of the oxygenator then an area A can be defined for every value of the flow fraction Ψ_Q, where the flow fraction is defined as $0 \leq \Psi_Q \leq 1$.

$$A(\Psi_Q) = \hat{x}, \hat{y} : Q(x, y) = \Psi_Q \times Q_{bc} \wedge \hat{x}, \hat{y} \subseteq x, y, \quad \forall x, y \in A_{CS} \tag{6}$$

The full data set for the cross-section is shown in Fig. 6 (Ψ_A, Ψ_Q) with $\Psi_A = \frac{A(\Psi_Q)}{A_{CS}}$. Note that the graph is a reflection on how uniformly the flow is distributed across the cross-section of the oxygenator. This is illustrated by a snap-shot of mass flow to area ratio at 70% in Fig. 7. The simulations show that large flow channels absorb most of the flow. For the device SRD3078 70% mass flow goes through only 10% area of the cross-section whereas the uniform arrangement of fibres in the idealised geometry yields a much more even mass flow versus area ratio. It can be further seen that the distribution of the fibres within the device has little impact on the flow directionality as mass flow versus area remain the same. Figs. 6 and 7 highlight the impact of a non-uniform distribution of fibres within the oxygenator.

The pressure drop however is flow rate and direction dependent. Eight experiments on three different builds of this prototype model are conducted. With an average flow rate of 380 mL min^{-1} a mean pressure drop of 3792 Pa is measured. The computational model for SRD3078 shows good agreement with 4053 Pa and 3853 Pa [R]everse. As these devices have all been manually assembled, they have potentially large flow channels as shown in Fig. 7. SRD3083 (with spacers) has a calculated pressure drop of 6443 Pa and 6218 Pa [R] and the idealised geometry 10,186 Pa. The pressure drop for 5 mL min^{-1} varies between 40 Pa and 220 Pa, but there is no experimental data available to compare with.

Cross-flow coefficients (O_{cf}) for all devices and flow rates are depicted in Fig. 8. Results are extracted at 14 cross-sections throughout the main body of the oxygenators at locations corresponding to the mesh elements. Increased cross-flow activity is visible close to inlet and outlet and is dependent on flow rate and fibre distribution. Due to a grid refinement at the inlet/outlet Eq. (5) is bound to overestimate O_{cf} and needs to be accounted for. The data suggest that decreasing the uniformity of fibres (SRD3078) leads to flow direction dependency whereas a uniform fibre distribution has the same O_{cf} in both directions.

With Eq. (2) and setting $d = 10\,\mu$m (representative of the size of capillaries in the human lung) we can calculate the shunt fraction O_{sf} for each device (see Table 3). The physical layout of the devices support flow parallel to the fibres, but as shown in Fig. 8 cross-flow is present. A parameter to adjust O_{sf} should be imposed to account for the cross-flow; otherwise Eq. (2) is overestimating the dead space. We propose to use O_{cf} as a relaxation factor for the shunt fraction O_{sf} (Eq. (7)).

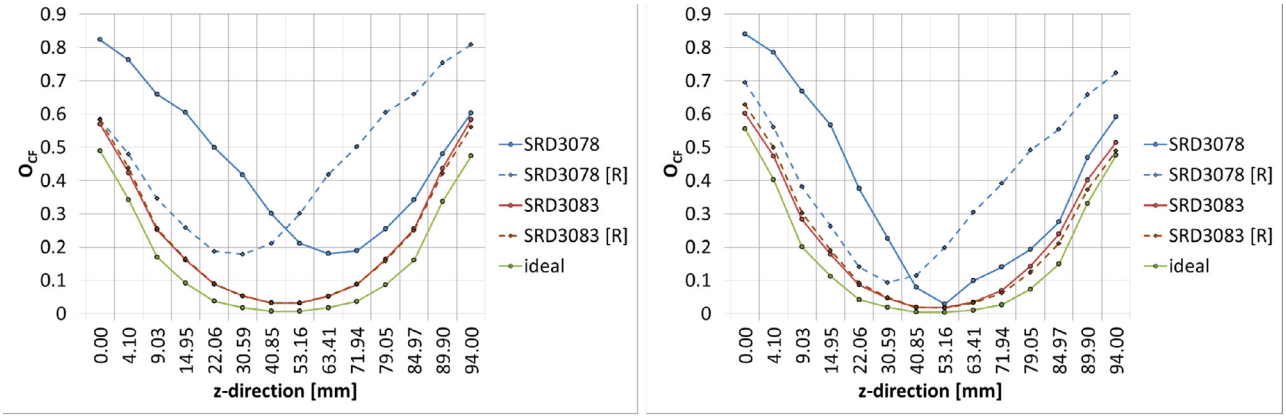

(a) 5 mL min^{-1} (b) 380 mL min^{-1}

Fig. 8. O_{cf} calculated at cross-sections corresponding to the mesh elements in z-direction.

Table 3
Shunt fractions independent of (O_{sf}) and dependent on (O_{sf^*}) q (flow rate).

				q = 5 mL min^{-1}		q = 380 mL min^{-1}	
Device	V_b	V_{b^*}	O_{sf}	O_{cf}	O_{sf^*}	O_{cf}	O_{sf^*}
SRD3078	13.1891	0.6224	0.9528	0.4520	0.5221	0.3815	0.5893
SRD3078 [R]	13.1891	0.6224	0.9528	0.4493	0.5247	0.3979	0.5737
SRD3083	12.3302	0.6506	0.9472	0.2278	0.7314	0.2221	0.7369
SRD3083 [R]	12.3302	0.6506	0.9472	0.2273	0.7319	0.2207	0.7382
Idealised	8.9593	0.6273	0.9300	0.1627	0.7787	0.1722	0.7698

Table 4
Streamline (S_l) in seconds and standard residence (τ) time in seconds for flow rate q.

	q = 5 mL min^{-1}				q = 380 mL min^{-1}			
Device	$S_l min$	$S_l max$	$S_l med$	τ	$S_l min$	$S_l max$	$S_l med$	τ
SRD3078	18.83	283.50	41.21	158.27	0.25	0.42	0.34	2.08
SRD3078 [R]	19.89	30.76	24.43	158.27	0.34	0.46	0.39	2.08
SRD3083	31.09	111.57	78.36	147.96	0.42	1.48	1.15	1.95
SRD3083 [R]	35.71	119.66	89.16	147.96	0.64	1.55	1.19	1.95
Idealised	70.74	86.68	78.99	107.51	0.85	1.08	0.97	1.41

$$O_{sf^*} = 1 - \frac{V_{b^*} + \left(O_{cf} * (V_b - V_{b^*})\right)}{V_b} \tag{7}$$

Thus we can account for a device dependent flow behaviour occurring from different fibre arrangements as well as for different flow rates. Table 3 lists the improved shunt fractions. The lower limit of O_{sf^*} is V_b whereas the upper limit is defined by V_{b^*}. The blood volume around the fibres being oxygenated, V_{b^*}, is adjusted by the distance d (see Eq. (2)) and needs to be chosen such that $V_{b^*} \leq V_b$.

Residence time of blood within the oxygenator was calculated in two ways; (i) by extracting streamlines (S_l) from the numerical solution and (ii) by the generic equation for residence time $\tau = V/q$ with $V = V_b$ and $q = Q_d$, set to the corresponding flow rate. The standard residence time is valid for steady laminar flow only. Reynolds number extracted for the numeric models are $R_e < 1$ for 5 mL min^{-1} flow rate and $R_e < 80$ for 380 mL min^{-1} hence flow can be assumed laminar. Streamlines were extracted in the main body of the oxygenator starting from 1000 equally spaced seed points. For the results in Table 4 only the streamlines reaching the outlet ($n > 95\,\%$ for all data sets) are considered. Fig. 9a and b depicts the streamline time distribution for two different flow rates. For better visualisation, only data points $\leq S_l med$ (median) are plotted. The bin size for 5 mL min^{-1} flow rate is 1 s and for 380 mL min^{-1} 0.01 s. Standard residence time in seconds (s) for 5 mL min^{-1} is calculated with $\tau = (V_b \times 60)/5$ and for 380 mL min^{-1} with $\tau = (V_b \times 60)/380$. The results are listed in Table 4.

4. Discussion

The presented μCT scans provide a feasible way to reconstruct an HFM-oxygenator with computer-aided design software (CAD) based on individual hollow fibres. The geometry can subsequently be used to run CFD models to study relevant design parameters for blood oxygenators. As an example our model shows the insensitivity of flow direction in regards to mass flow versus area but highlights the importance of a uniform fibre distribution. In the case of SRD3078 70% of blood is flowing through the device with very little contact to fibres, suggesting limited oxygenation efficiency (Fig. 7). By comparing pressure drops and residence times we can highlight the dependency on flow direction.

Especially residence time of blood is an important factor in the design of a blood oxygenator, to provide optimal mass transfer and blood oxygen saturation. We have shown that residence time based on velocity vectors (streamlines) in a full scale model reveal a distribution which cannot be represented by the standard equation for fluid resident time in a reservoir (Table 4 and Fig. 9). According to Kang et al. [12] the time of oxygen saturation of red blood cells is between 60 ms (rest) and 120 ms (exercise). This time scale is at least a magnitude shorter than the minimum residence time

Please cite this article as: C. D'Onofrio et al., Three-dimensional computational model of a blood oxygenator reconstructed from micro-CT scans, Medical Engineering and Physics (2017), http://dx.doi.org/10.1016/j.medengphy.2017.06.035

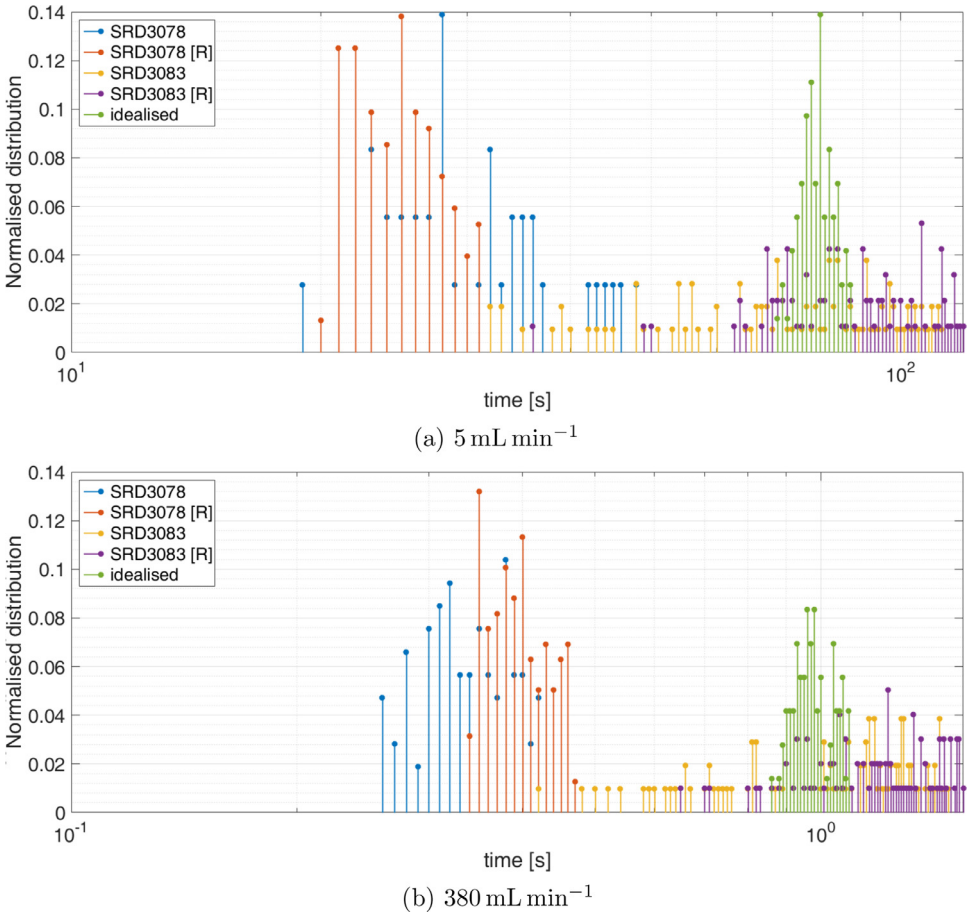

Fig. 9. Distribution of streamline residence time in the main body of the oxygenator. For a better visualisation the graph depicts only data ≤ the median. (a) has a bin size of 1 s and (b) has a bin size of 0.01 s.

of blood in the studied oxygenator. Hence our results suggest that even with a significantly reduced length of the main body of the oxygenator sufficient oxygenation and a potential decrease of the device's thrombogenicity could be achieved.

Furthermore we have presented a method to quantitatively assess cross-flow activity and a device dependent shunt fraction. Despite the prototypes physically supporting longitudinal flow, we could reveal cross-flow activity probably due to the positioning of the blood inlet and outlet tube and a non-uniform distribution of fibres. Oxygenator shunt fraction, O_{sf*}, takes flow rate, direction and cross-flow activity into account and can be adjusted using a single parameter d to describe the blood volume being oxygenated. We have used a nominal value of $d = 10\,\mu m$ to reflect human capillaries, but this may be different for other hollow fibre membrane oxygenators and needs further investigation. Combined they show the potential as a qualitative design optimization parameter.

So far, to the best of our knowledge, the existing literature reports studies with a porous zone or a uniformly distributed arrangement of fibres to model the blood flow through the oxygenator. Using either method assumes a homogeneous uniform permeability or a pre-calculated permeability based on a uniform distribution of fibres. In this study, we have shown that such a distribution of fibres is unlikely and even a small variability in gap size between the fibres changes the flow behaviour significantly.

5. Conclusions

μCT scans provide a feasible tool to rebuild the geometry of a hollow fibre membrane oxygenator. We have shown how to quantitatively and qualitatively assess prototype oxygenators and can conclude that a significant change in transport phenomena and mass exchange is to be expected if large gaps between fibres are present, i.e. uniform distribution of fibres are paramount for blood oxygenators.

To solve a full scale meshed oxygenator is computationally more expensive than a porous media approach, but yields an insight into the oxygenator otherwise not achievable. We were able to solve the flow problem on the model presented (~20 million cells) within 24 h on a single workstation computer (Xeon E3-1240 v3, 4 cores at 3.4 GHz, 16 GB RAM).

We have shown the capability of using a full scale three-dimensional numerical model to realistically simulate flow behaviour using accurate geometrical descriptions of the oxygenator rather than idealised geometries. As the boundaries of the fibres are accurately meshed, further analysis of mass transfer is possible by solving a convection-diffusion problem based on the flow solutions in this work. The reconstruction of individual fibres for example, could be used to apply the transport models presented by Taskin et al. [23] to calculate individual P_{O_2} profiles and study the mass exchange in detail. Such a model is therefore a feasible tool to study design optimisations of HFM oxygenators and may facilitate the development of a wearable ECMO device and/or an implantable artificial lung.

Conflict of interest

None declared.

Please cite this article as: C. D'Onofrio et al., Three-dimensional computational model of a blood oxygenator reconstructed from micro-CT scans, Medical Engineering and Physics (2017), http://dx.doi.org/10.1016/j.medengphy.2017.06.035

Ethical approval

Not required.

Acknowledgements

The authors would like to acknowledge the Advanced Sustainable Manufacturing Technologies (ASTUTE) project, part-funded by the European Regional Development Fund through the Welsh Government as well as the assistance provided by the Swansea University AIM Facility, which was funded in part by the EPSRC (EP/M028267/1), the European Regional Development Fund through the Welsh Government (80708) and the Ser Solar project via Welsh Government.

Supplementary material

Supplementary material associated with this article can be found, in the online version, at 10.1016/j.medengphy.2017.06.035.

References

[1] ANSYS Inc. ®, Ansys academic research – fluent. Simulation-Driven Product Development. URL http://www.ansys.com/. 2013.
[2] Berggren SM. The oxygen deficit of arterial blood caused by non-ventilating parts of the lung. Johnson Repr. Corporation; 1964.
[3] Bhavsar SS, Schmitz-Rode T, Steinseifer U. Numerical modeling of anisotropic fiber bundle behavior in oxygenators. Artif Organs 2011;35(11):1095–102. doi:10.1111/j.1525-1594.2011.01365.x.
[4] Chatburn RL, Volsko TA, Hazy J, Harris LN, Sanders S. Determining the basis for a taxonomy of mechanical ventilation. Respir Care 2012;57(4):514–24. doi:10.4187/respcare.01327.
[5] Consolo F, Fiore GB, Pelosi A, Reggiani S, Redaelli A. A numerical performance assessment of a commercial cardiopulmonary by-pass blood heat exchanger. Med. Eng. Phys. 2015;37(6):584–92. http://dx.doi.org/10.1016/j.medengphy.2015.03.002.
[6] Gartner MJ, Wilhelm CR, Gage KL, Fabrizio MC, Wagner WR. Modeling flow effects on thrombotic deposition in a membrane oxygenator. Artif Organs 2000;24(1):29–36. doi:10.1046/j.1525-1594.2000.06384.x.
[7] GOV.UK, Medicines & healthcare products regulatory agency UK, Online, page visited 2016-09, 2016, https://www.gov.uk/government/organisations/medicines-and-healthcare-products-regulatory-agency.
[8] Haworth WS. The development of the modern oxygenator. Ann Thoracic Surg 2003;76(6):S2216–19. doi:10.1016/j.athoracsur.2003.09.012.
[9] Hormes M, Borchardt R, Mager I, Rode TS, Behr M, Steinseifer U. A validated cfd model to predict O_2 and CO_2 transfer within hollow fiber membrane oxygenators. Int J Artif Organs 2011;34(3):317–25. http://europepmc.org/abstract/MED/21462147
[10] HSE. Health and safety executive. Chronic obstructive pulmonary disease (copd)2015. Online. http://www.hse.gov.uk/statistics/causdis/copd/.
[11] Johnston BM, Johnston PR, Corney S, Kilpatrick D. Non-Newtonian blood flow in human right coronary arteries: steady state simulations. J Biomech 2004;37(5):709–20. http://dx.doi.org/10.1016/j.jbiomech.2003.09.016.
[12] Kang M-Y, Katz I, Sapoval B. A new approach to the dynamics of oxygen capture by the human lung. Respir Physiol Neurobiol 2014;205:109–19. doi:10.1016/j.resp.2014.11.001.
[13] Khanafer KM, Cook K, Marafie A. The role of porous media in modeling fluid flow within hollow fiber membranes of the total artificial lung. J PorousMedia 2012;15(2):113–22.
[14] Low KWQ, van Loon R, Rolland SA, Sienz J. Pore-scale modeling of non-Newtonian shear-thinning fluids in blood oxygenator design. J Biomech Eng–Trans ASME 2016;138(5). doi:10.1115/1.4032801.
[15] Marcinkowska-Gapińska A, Gapinski J, Elikowski W, Jaroszyk F, Kubisz L. Comparison of three rheological models of shear flow behavior studied on blood samples from post-infarction patients. Med Biol Eng Comput 2007;45(9):837–44. doi:10.1007/s11517-007-0236-4.
[16] Mazaheri AR, Ahmadi G. Uniformity of the fluid flow velocities within hollow fiber membranes of blood oxygenation devices. Artif Organs 2006;30(1):10–15. doi:10.1111/j.1525-1594.2006.00150.x.
[17] Membrana GmbH, Oxyplus, Internet, 2013, http://www.membrana.com/healthcare/products/blood-oxygenation-products/oxyplus.
[18] Nagase K, Kohori F, Sakai K. Oxygen transfer performance of a membrane oxygenator composed of crossed and parallel hollow fibers. Biochem Eng J 2005;24(2):105–13. http://dx.doi.org/10.1016/j.bej.2005.02.003.
[19] NHS. National health service. Chronic obstructive pulmonary disease health (copd).2013. Online, page visited August 2013, page last updated February 2013. http://www.nhsinform.co.uk/health-library/articles/c/chronic-obstructive-pulmonary-disease/introduction.
[20] Pelosi A, Sheriff J, Stevanella M, Fiore GB, Bluestein D, Redaelli A. Computational evaluation of the thrombogenic potential of a hollow-fiber oxygenator with integrated heat exchanger during extracorporeal circulation. Biomech Model Mechanobiol 2014;13(2):349–61. doi:10.1007/s10237-012-0445-0.
[21] Quemada D. Rheology of concentrated disperse systems ii. a model for non-Newtonian shear viscosity in steady flows. Rheol Acta 1978;17(6):632–42.
[22] Schindelin J, Arganda-Carreras I, Frise E, Kaynig V, Longair M, Pietzsch T, et al. Fiji: an open-source platform for biological-image analysis. Nat Methods 2012;9(7):676–82. doi:10.1038/nmeth.2019.
[23] Taskin ME, Fraser KH, Zhang T, Griffith BP, Wu ZJ. Micro-scale modeling of flow and oxygen transfer in hollow-fiber membrane bundle. J Membrane Sci 2010;362(1–2):172–83. doi:10.1016/j.memsci.2010.06.034.
[24] WBS The Welsh blood service covers the whole of wales collecting voluntary, non-remunerated blood donations from the general public. Online, page visited 2016-09. URL https://www.welsh-blood.org.uk/about-us/; 2016.
[25] Zhang J, Nolan TD, Zhang T, Griffith BP, Wu ZJ. Characterization of membrane blood oxygenation devices using computational fluid dynamics. J Membrane Sci 2007;288(1):268–79. doi:10.1016/j.memsci.2006.11.041.